Benchmarking and procrustean noise reduction of entangled mixed states

Peters, Nicholas, Wei, Tzu-Cheih, Kwiat, Paul

Nicholas A. Peters, Tzu-Cheih Wei, Paul G. Kwiat, "Benchmarking and procrustean noise reduction of entangled mixed states," Proc. SPIE 5468, Fluctuations and Noise in Photonics and Quantum Optics II, (25 May 2004); doi: 10.1117/12.546857

SPIE.

Event: Second International Symposium on Fluctuations and Noise, 2004, Maspalomas, Gran Canaria Island, Spain

Benchmarking and Procrustean noise reduction of entangled mixed states

Nicholas A. Peters, Tzu-Chieh Wei, and Paul G. Kwiat

Physics Department, University of Illinois, 1110 West Green Street, Urbana, IL 61801, U.S.A.

ABSTRACT

Understanding quantum noise is essential for accurately creating desired quantum states and for examining a given state's evolution in any protocol. Using spontaneous parametric downconversion, we can create a wide variety of single- and two-qubit polarization states, including nearly perfect Bell states, mixed states (i.e., "noisy" states) and maximally entangled mixed states (MEMS). To characterize these states we use several different measures, including fidelity, "tangle" and linear entropy. In the course of our experiments, we have discovered and numerically investigated an extreme imbalance in the sensitivity of these different two-qubit state measures. We have also experimentally realized a "Procrustean" filtering technique to remove noise from MEMS. For moderate amounts of filtering, the experimental procedure works as desired to increase the tangle and decrease the linear entropy. However, for large amounts of filtering, the process becomes dominated by perturbations in the starting density matrix. The final outcome is a pure (i.e., zero entropy) product state (i.e., zero entanglement).

Keywords: SPDC, MEMS, entanglement, Procrustean filtering

1. INTRODUCTION

Many protocols, including provably secure cryptography,[1,2] teleportation,[3] and super-dense coding,[4] have been proposed to exploit various properties of quantum mechanics to "process" information. These protocols and most others in quantum information processing require a fiducial initial quantum state. In the case of one- and two-qubit protocols, optimal results are generally obtained with pure states, while oftentimes two-qubit protocols additionally require high quality entanglement. However, decoherence and dissipation may cause the states to become mixed and/or less entangled. The success of such protocols often hinges on both the purity and the entanglement as, for example, in teleportation.[5] Using photonic qubits encoded in polarization, we can create a variety of one- and two-qubit states, allowing the exploration of mixed states in two Hilbert-space dimensions. In both cases, we examine the influence of noise modeled with a depolarizing channel, i.e., adding a completely mixed state incoherently to the states we study. Using the fidelity,[6] we set quantitative bounds on the induced depolarization and compare the sensitivity of different states and different measures to changes in the noise.

2. MEASURES

We measure the overall noise with the linear entropy[5] (S_L), and for two-qubit states we also quantify entanglement using the tangle[7,8] (T). We choose the linear entropy because it is based on the purity, i.e., $\propto Tr(\rho)^2$, and the tangle because it is based on the concurrence, which has a simple form for the class of states we consider. The linear entropy is given by

$$S_L(\rho) \;=\; \mathcal{N}_i[1 - Tr(\rho^2)], \tag{1}$$

Send correspondence to N.A.P.
E-mail: npeters@uiuc.edu, Telephone: 1 217 244 1608

Fluctuations and Noise in Photonics and Quantum Optics II, edited by Peter Heszler, Derek Abbott, Julio R. Gea-Banacloche, Philip R. Hemmer, Proceedings of SPIE Vol. 5468 (SPIE, Bellingham, WA, 2004) 0277-786X/04/$15 · doi: 10.1117/12.546857

where $\mathcal{N}_i$ is a normalization factor which is $\mathcal{N}_1 = 2$ for one-qubit states and $\mathcal{N}_2 = \frac{4}{3}$ for two-qubit states. The linear entropy ranges from zero for pure states to one for the maximally mixed state, i.e., a normalized identity. The tangle is given by

$$T(\rho) \;=\; C^2, \tag{2}$$

where $C = max\{0, \lambda_1 - \lambda_2 - \lambda_3 - \lambda_4\}$ is the concurrence and λ_i are the square roots of the eigenvalues of $\rho(\sigma_2 \otimes \sigma_2)\rho^*(\sigma_2 \otimes \sigma_2)$, in non-increasing order by magnitude, with $\sigma_2 = \begin{pmatrix} 0 & -i \\ i & 0 \end{pmatrix}$. The tangle is zero for product states and one for maximally entangled states, e.g., Bell states.

For direct comparison of two different states, e.g., a measured state $|\psi_m\rangle$ and a target state $|\psi_t\rangle$, we use the fidelity, a measure of the state overlap $|\langle\psi_m|\psi_t\rangle|^2$. For more general mixed states ρ_m and ρ_t, the fidelity[6] is given by

$$F(\rho_t, \rho_m) \equiv \left| \mathrm{Tr}\left(\sqrt{\sqrt{\rho_t}\rho_m\sqrt{\rho_t}} \right) \right|^2. \tag{3}$$

In either case, the fidelity is zero for orthogonal states and one for identical states.

3. ONE QUBIT

We start our exploration of noise effects with the simple two-level quantum system–a qubit. In this manuscript, we will represent our qubits as photon polarization states in the horizontal-vertical bases:

$$|0\rangle \equiv |H\rangle \equiv \begin{pmatrix} 1 \\ 0 \end{pmatrix} \text{ and } |1\rangle \equiv |V\rangle \equiv \begin{pmatrix} 0 \\ 1 \end{pmatrix}, \tag{4}$$

or in density matrix notation,

$$\rho_H = \begin{pmatrix} 1 & 0 \\ 0 & 0 \end{pmatrix} \text{ and } \rho_V = \begin{pmatrix} 0 & 0 \\ 0 & 1 \end{pmatrix}. \tag{5}$$

However, all of our findings are directly applicable to *any* two-level system, and thus have relevance for all physical qubit realizations.

The density matrix of an arbitrary single qubit can be represented by three independent real parameters (A, B, and δ):

$$\rho = \begin{pmatrix} A & Be^{i\delta} \\ Be^{-i\delta} & 1-A \end{pmatrix}, \tag{6}$$

where $0 \leq \mathrm{A} \leq 1$ from normalization, and $|B| \leq \sqrt{A(1-A)}$ from positive semi-definiteness. We are able to create arbitrary states[9] of equation (6) using the minimum number of varying elements (three), two half-waveplates (HWP) and a quarter-waveplate (QWP) as shown in figure 1 (a). Shown in part (b) is a typical created state along with its target and the fidelity between the target state and the measured state.

To understand the influence of noise on a single-qubit state, we consider the pure state $|\theta\rangle = \cos 2\theta|H\rangle + \sin 2\theta|V\rangle$ when acted on by a depolarizing channel:

$$\rho_{d,1}(\lambda, \theta) = (1-\lambda)|\theta\rangle\langle\theta| + \frac{\lambda}{2}\mathbf{I}_1, \tag{7}$$

where $\mathbf{I_1}$ is the two-by-two identity and λ is the strength of the depolarization (added noise). This mixed state is the "benchmark" state, and we examine the effect of small changes in λ. From (1), the qubit's linear entropy is

$$S_L(\rho_{d,1}(\lambda, \theta)) = 2\lambda - \lambda^2, \tag{8}$$

depending only on the strength of depolarization because the state $|\theta\rangle$ is pure. As the parameter θ does not affect the linear entropy, without loss of generality we set θ=0. To bound the variation in the depolarized

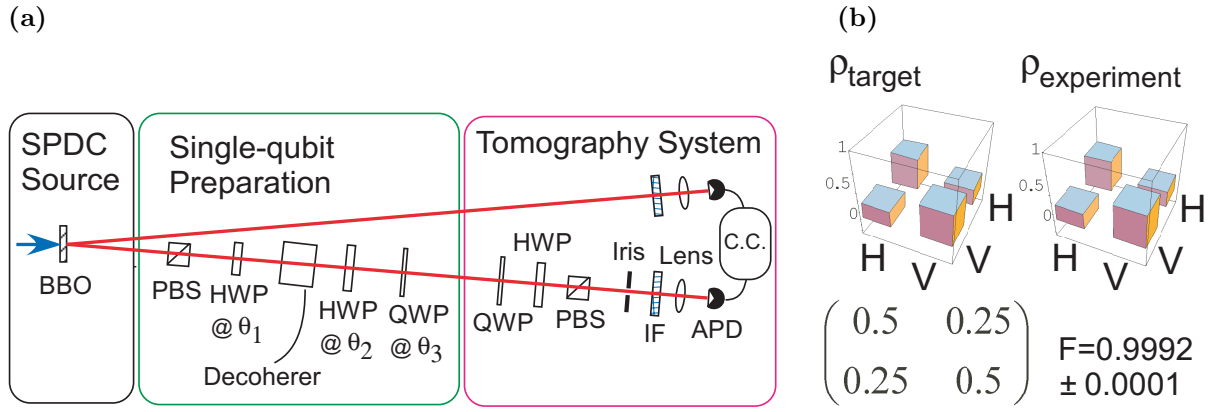

Figure 1. Single-qubit downconversion experiment and data. (a) Single qubit experiment. Single-photon states are conditionally prepared[10] in the lower arm by detecting a trigger photon in the upper arm with an avalanche photodiode (APD). The single-photon qubit and its trigger are a two-photon pair produced with a nonlinear BBO crystal. The polarizing beam splitter (PBS) prepares a pure initial state $|H\rangle$, which is transformed by the waveplates and decoherer (∼1 cm quartz birefringent element) into an arbitrary polarization state. The tomography system uses a quarter-waveplate (QWP), HWP, and a PBS to analyze in arbitrary polarization bases, allowing accurate state measurement. (b) Single qubit data. Shown is a typical target density matrix and the corresponding experimental measurement. Also shown are the numeric target and the target-measured fidelity (F). Not shown are the imaginary elements of the density matrix as they are zero for this target and less than 2% for the measured state.

state behavior, we calculate the fidelity between the initial "target state" $\rho_{d,1}(\lambda, 0)$ and a slightly perturbed state $\rho_{d,1}(\lambda + \delta\lambda, 0)$:

$$F(\rho_{d,1}(\lambda,0), \rho_{d,1}(\lambda+\delta\lambda,0) = \frac{1}{4}(\sqrt{(\lambda-2)(\lambda+\delta\lambda-2)} + \sqrt{\lambda(\lambda+\delta\lambda)})^2. \tag{9}$$

We then solve for the variation $\delta\lambda$ that produces a given level of fidelity:

$$\delta\lambda_{\pm}(\lambda, \mathrm{F}) = 2(1 - \mathrm{F} - \lambda + \mathrm{F}\lambda \pm \sqrt{\mathrm{F}(1-\mathrm{F})(2\lambda - \lambda^2)}). \tag{10}$$

In this way we generate a series of states that have a specified fidelity with the target state, and then ask how the linear entropy (S_L) changes. For example, $S_L(\lambda)$, $S_L(\lambda + \delta\lambda_+)$ and $S_L(\lambda + \delta\lambda_-)$ are plotted in figure 2 for a fidelity of 0.99 (typically considered "high fidelity") as a function of λ. Note that for both a completely pure state (λ=0) and a completely mixed state (λ=1), $\delta\lambda_+$ and $\delta\lambda_-$ have the same magnitude; thus the linear entropy increases by 0.0396 for the pure state, and decreases by the same amount for the mixed state). In other words, the pure state *de*polarizes while the mixed state *re*polarizes to reach a 0.99 fidelity. When the target is a pure state, a ∼4% linear entropy increase can occur and still have 0.99 fidelity with the initial pure state. Things are much worse for partially mixed states. For example, the linear entropy is 0.75 for $\lambda = 0.5$, but the 0.99 fidelity states have linear entropies of 0.90 (depolarized dashed line of figure 2) and 0.56 (repolarized dotted line).

Thus we see that the sensitivity of S_L to perturbations in the input state depends critically on the entropy of the starting state itself. When we perturb an initial state with parameter λ by $\delta\lambda_+$ and $\delta\lambda_-$, we see how much the linear entropy can change while maintaining a constant fidelity between the initial and perturbed states. While this bound creates a curve for a continuum of states based on the parameter λ, we shall see in section 4 when we consider the tangle and linear entropy for two-qubit states, that we can map the behavior with more flexibility than that of the two points provided by $\delta\lambda_+$ and $\delta\lambda_-$.

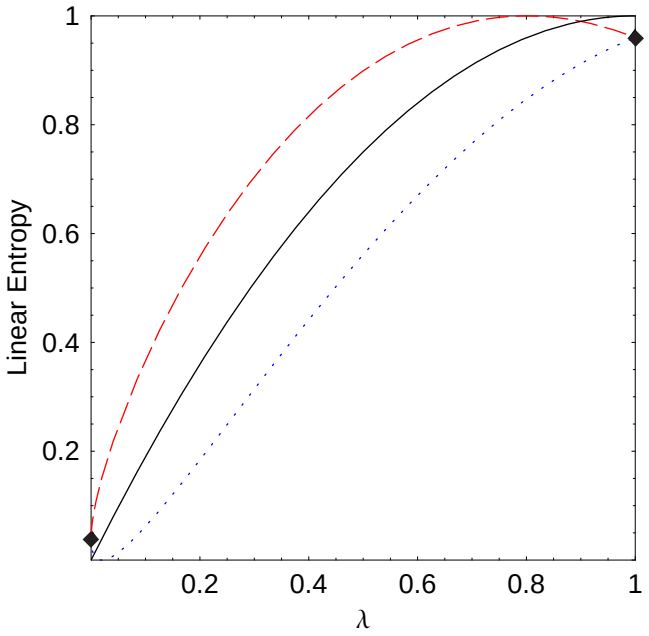

Figure 2. The linear entropy of a depolarized single qubit state $|H\rangle$ as a function of an applied depolarizing channel (λ) (see (7)). The solid line is the linear entropy for the state $\rho_{d,1}(\lambda, 0)$ while the dashed and dotted lines are curves for states that have 0.99 fidelity with $\rho_{d,1}(\lambda)$. The dashed and dotted lines are for the states $\rho_{d,1}(\lambda + \delta\lambda_+)$ and $\rho_{d,1}(\lambda + \delta\lambda_-)$ respectively. Diamonds at λ=0 and λ=1 show where the dashed and dotted lines touch (see text). When the dashed and dotted lines are above the solid line, they exhibit *de*polarizing behavior; when they are below the solid line, they exhibit *re*polarizing behavior.

4. TWO QUBITS

In this section, we will consider two-qubit states, the minimal system that displays entanglement. There are several classes of two-qubit entangled states; maximally and nonmaximally entangled pure states,[11–13] nonmaximally entangled mixed states,[14] and the special case of Werner states[15] (an incoherent combination of a mixed state and a pure maximally entangled state), all of which have been experimentally realized with polarization qubits. While for some time it was thought that Werner states were maximally entangled for a given mixture, Munro et al. discovered a class of states more entangled than Werner states of the same linear entropy,[16] the maximally entangled mixed states (MEMS). MEMS possess the *maximum* tangle for a given amount of linear entropy*. They exist in two subclasses, ρ_{MEMSI} and ρ_{MEMSII}, possessing two and three eigenvalues, respectively:

$$\rho_{MEMS\ I} = \begin{pmatrix} \frac{r}{2} & 0 & 0 & \frac{r}{2} \\ 0 & 1-r & 0 & 0 \\ 0 & 0 & 0 & 0 \\ \frac{r}{2} & 0 & 0 & \frac{r}{2} \end{pmatrix}, \quad \frac{2}{3} \leq r \leq 1, \quad \text{and} \tag{11}$$

*For certain mixedness-entanglement parameterizations, however, the Werner states *are* the states which possess the maximal amount of entanglement for a given degree of mixedness, i.e., the Werner states *are* the MEMS.[17]

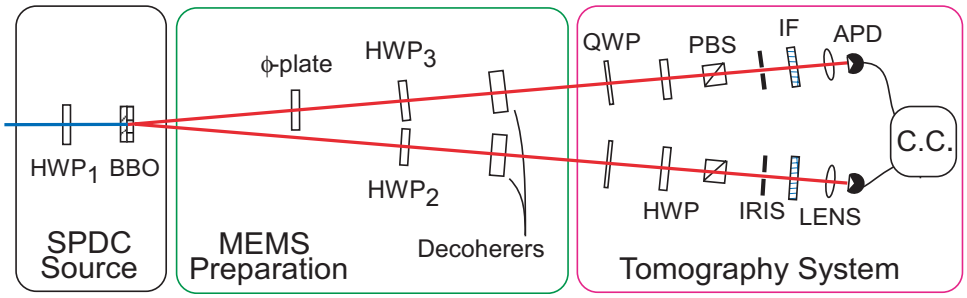

Figure 3. MEMS creation experiment. A half-waveplate (HWP_1) sets the pure state's initial entanglement. Then the relative phase between $|HH\rangle$ and $|VV\rangle$ is set to zero using a ϕ-plate (a QWP tipped about its vertical optic axis). The state is rotated into the active bases of the decoherers with HWP_2 and HWP_3, thereby adjusting the state entropy. The tomography system is simply two copies of the one-qubit analysis system, using a QWP, HWP, and a polarizer in each arm to analyze in arbitrary polarization bases. Transmitted photons are counted in coincidence via avalanche photodiodes.

$$\rho_{MEMS\ II} = \begin{pmatrix} \frac{1}{3} & 0 & 0 & \frac{r}{2} \\ 0 & \frac{1}{3} & 0 & 0 \\ 0 & 0 & 0 & 0 \\ \frac{r}{2} & 0 & 0 & \frac{1}{3} \end{pmatrix}, \quad 0 \le r \le \frac{2}{3}, \tag{12}$$

where it can be shown that the parameter r is the concurrence of the state. Note that $r = 1$ gives the maximally entangled Bell state $(|HH\rangle + |VV\rangle)/\sqrt{2}$.

4.1. State Creation

We have recently created MEMS states,[18,19] accessing the last unexplored region of linear entropy-tangle state space. MEMS creation involves three steps: creating the initial pure entangled state, applying local unitary transformations, and decohering. Spontaneous parametric downconversion is used to create frequency degenerate 702-nm photons, generated by pumping thin BBO crystals with an Ar-ion laser at 351 nm. Polarization entanglement results from pumping two such crystals oriented with their optic axes in perpendicular planes. The pump polarization is set with $\mathrm{HWP}_1 = \theta_1$, as in figure 3. This creates a state of variable entanglement,

$$|\Psi(\theta)\rangle \equiv \cos 2\theta_1 |HH\rangle + \sin 2\theta_1 |VV\rangle, \tag{13}$$

where $|HH\rangle$ ($|VV\rangle$) represents two horizontally (vertically) polarized photons.[12,13]

The initial entanglement is set to that of the MEMS I target state (the creation of MEMS II proceeds slightly differently and is discussed below). After the initial entanglement is set, a maximum likelihood tomography[13,20] of it is taken and used to numerically find the settings of HWP_2 and HWP_3 (see figure 3) that give the desired predecohered state. These waveplates set the diagonal elements of the predecohered state to those of the target MEMS I. The MEMS is sensitive to not only the waveplate settings, but also to their birefringent retardations, which are measured and used in the aforementioned numerical calculation.

After the waveplates, the state photons pass through birefringent decoherers, which reduce specific off-diagonal elements of the density matrix, i.e., they decohere in a specific basis yielding the MEMS I state[†]. Each decoherer is a ∼1-cm thick piece of quartz with a horizontally oriented optic axis. The thickness is chosen so that the polarization-dependent optical path length difference ($\sim 140\lambda$) is larger than the downconversion coherence length ($L_c \equiv \lambda^2/\Delta\lambda \cong 70\lambda$), determined by a 10-nm FWHM interference filter

[†]As recently demonstrated,[21,22] one could instead uses the spatial degree of freedom to decohere, but then the states would not be suitable for some purposes such as those requiring fiber optics or interference methods.

placed before each detector. Because the optical path length difference of the decoherers is not exactly 140λ, an additional phase on the MEMS off-diagonal elements is introduced. We correct for the additional phase by slightly tipping one of the decoherers.

The decoherers couple the polarization with the relative arrival times of the photons.[9, 23] While detection of two horizontal ($|HH\rangle$) or vertical ($|VV\rangle$) photons will be simultaneous, photons in the state $|HV\rangle$ would in principle be detected first in arm # 1 and second in arm # 2 (assuming the decoherer slows vertically polarized photons relative to horizontally polarized photons). Detection would occur in the opposite order for the state $|VH\rangle$.

After the decoherers, the state is analyzed with a tomography system (see figure 3). A quarter-waveplate (QWP), HWP, and polarizing beam splitter (PBS) in each arm allow analysis by projecting into arbitrary polarization states. The tomography system projects the two-photon state into 16 different polarization states, e.g, $\langle HH|$, $\langle HV|$, etc. The results are then processed by a maximum likelihood tomography[20] technique to determine the state most likely to have produced the observed data.

MEMS II are created by first creating the MEMS I state with $r = 2/3$, the border state between the two subclasses. To travel along the MEMS II curve, the optical path length difference on one arm must be varied from 140λ. When one decoherer is changed, different relative timings are coupled to $|HH\rangle$ and $|VV\rangle$, inducing decoherence between them. For example, to make the MEMS II state shown in figure 4 (a), a 140λ decoherer was used in one arm while a 90λ decoherer was used in the other.

Typical MEMS data is shown in figure 4. Target states are shown as stars while experimental states are boxes with error bars. Note that in all cases except for the Bell state ($\rho_{MEMSI}(r = 1)$), the experimental states do not overlap their targets although the measured density matrices have high fidelity (typically $\sim 99\%$). To understand this discrepancy, we generated numeric perturbations of the target states by first calculating expected ideal measurements. Perturbed values for these measurements are then generated as random numbers from Poisson distributions, using the expected ideal counts as the distribution mean. These Poisson perturbed values are then entered into the maximum likelihood program to give physically valid density matrices. The fidelity of the noisy matrices and the target states is calculated and if it is at least 0.99, the tangle and linear entropy is plotted about the target state. For each target state, 5000 such points were generated and are shown as dark shaded regions in figure 4 (a). Note that the perturbed states for the Bell state lie on the Werner state line. This reinforces the idea that random perturbations of state measurements (as is encountered in photon counting) may be modeled through a depolarizing channel.

To examine the change a depolarizing channel has on two-qubit states, we define the following:

$$\rho_1(\lambda, \theta) \equiv (1 - \lambda)|\Psi(\theta)\rangle\langle\Psi(\theta)| + \frac{\lambda}{4}\mathbf{I_2}, \quad \text{and} \tag{14}$$

$$\rho_2(\lambda, r) \equiv (1 - \lambda)\rho_{MEMSI}(r) + \frac{\lambda}{4}\mathbf{I_2}, \tag{15}$$

where $|\Psi(\theta)\rangle$ is the (partially-) entangled state from (13). Here λ is the depolarizing parameter, as it was for one-qubit, and $\mathbf{I_2}$ is the four-by-four identity matrix. We use (14) to explore the linear entropy-tangle plane along the Werner curve, and (15) to explore above it. The combination of the two styles of perturbation allows us to cordon off an entropy-tangle curve wherein lie states of a certain fidelity with the Bell state ($\rho_1(0, 22.5^\circ) = \rho_2(0, 1) = (|HH\rangle + |VV\rangle)/\sqrt{2}$). This analysis proceeds in the same way as it did for one qubit, but now including perturbations for both parameters, so that the tangle and entropy of the perturbed state change while the fidelity with the Bell state remains constant. Thus this type of perturbation is not entirely due to the depolarizing channel. We are not suggesting that this is the optimal scheme for modeling perturbations, but it is helpful for visualizing how the fidelity, linear entropy and tangle relate to each other for a specific class of states. One advantage to the parameterization of ρ_1 is that small changes of λ and θ independently affect the noise and entanglement respectively. However, because the equations are more complicated for the two-qubit case, we solved them numerically. The results for the Bell state are shown in figure 5. Depending on the underlying assumptions, fault-tolerant computing nominally requires less than

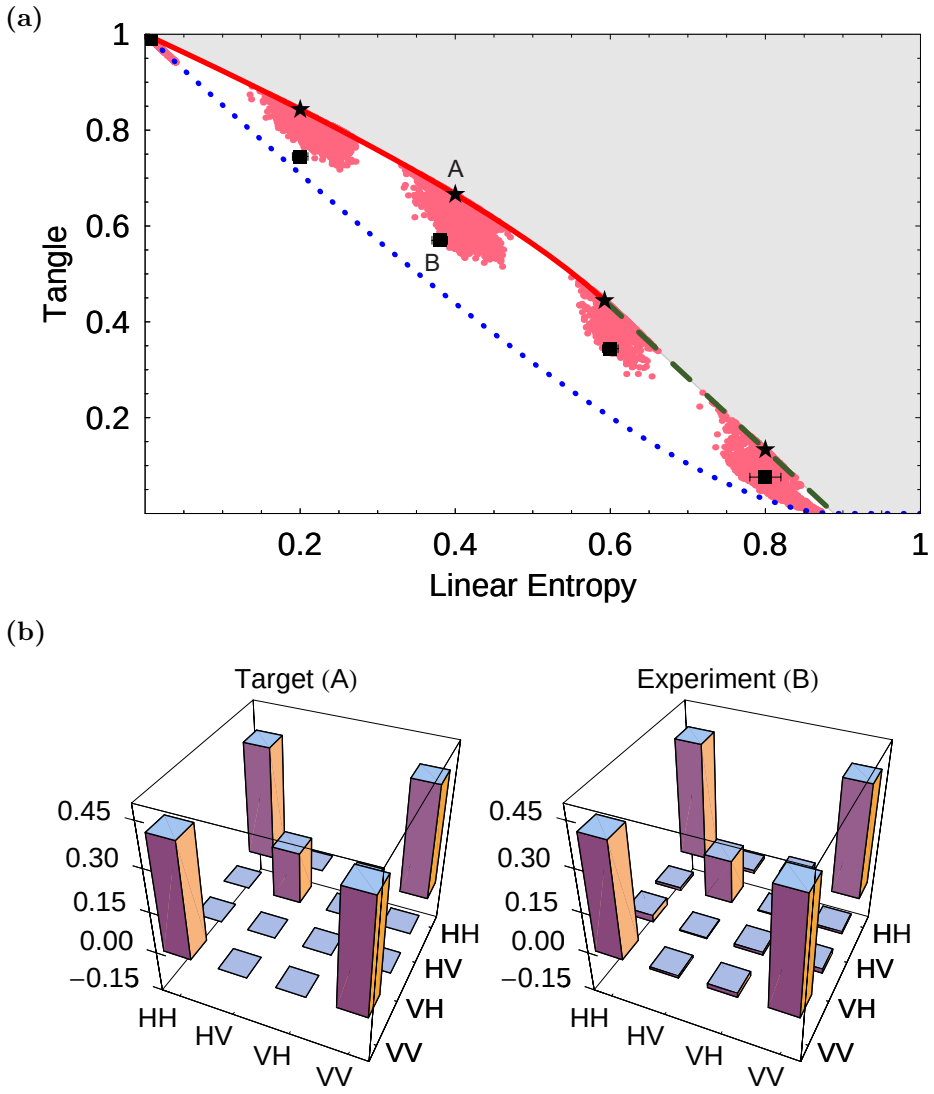

Figure 4. MEMS Data. (a) MEMS data on the Linear Entropy-Tangle plane (modified from Ref. 19). Theoretical curves are shown for MEMS I (solid line), MEMS II (dashed line) and Werner states (dotted line). The lightly shaded region beyond the MEMS theory curves is unphysical. Target states are shown with stars and the corresponding experimentally measured states shown as squares with error bars. Note that we are able to attain nearly perfect Bell states in the upper left corner of the plot. The shaded patches around each target state show the tangle and linear entropy for 5000 numerically generated states with a fidelity of at least 0.99 with the corresponding target. The perturbed Bell states closely resemble the behavior of depolarized Bell states because they lie on the Werner state theory curve. We attribute this behavior to the symmetry of the Bell state, namely that when perturbed with uniform (i.e., randomly distributed) noise, it is unlikely to reach the asymmetric form of the MEMS. (b) Density matrix plot for the real components of a MEMS I (r=0.8162, A) and the experimentally realized state (B) shown in (a). The imaginary components of the target state are negligible and are not shown because on average they are less than 0.005. The states in (b) agree well, with Fidelity 0.981 ± 0.003; the uncertainty is determined from a MonteCarlo simulation accounting for statistical fluctuations.

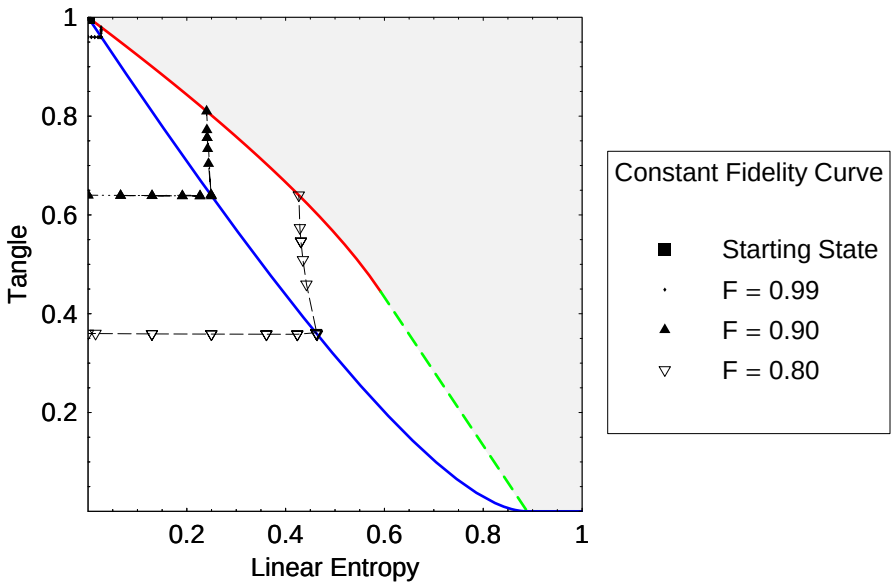

Figure 5. Constant fidelity curves for a maximally entangled state $(|HH\rangle + |VV\rangle)/\sqrt{2}$. The (essentially horizontal) constant fidelity curves below the Werner state curve are swept out by comparing the starting state with states of the form $\rho_1(\lambda, \theta)$, (14), while the (nearly vertical) curves above are generated by varying the parameters of $\rho_2(\lambda, r)$ (15).

$\sim 10^{-4}$ errors per gate.[24,25] To attain this level, a Bell state with noise modeled as in (14) must have tangle greater than 0.9996 and linear entropy less than 0.00027. To the best of our knowledge, this level is still beyond current technology.

While the Bell state is optimal as an entanglement resource, it is just one corner of the entropy-tangle plane. To investigate behavior "on the open plane," we examine an entangled mixed state that is a specific example of ρ_1:

$$\rho_1(\sim 0.225, \sim 11.57^\circ) \;=\; \begin{pmatrix} 0.7113 & 0 & 0 & 0.2800 \\ 0 & 0.0564 & 0 & 0 \\ 0 & 0 & 0.0564 & 0 \\ 0.2800 & 0 & 0 & 0.1760 \end{pmatrix}, \tag{16}$$

which is shown as the target in figure 6. Note that the 0.99 fidelity region is much larger here than for the Bell state. This seems to indicate that changing a pure state by adding noise alters the state characteristics (i.e., the tangle and linear entropy but not fidelity) much less than varying an already partially-mixed starting state, i.e., noisy states are more sensitive to these types of changes than pure states. Recall that we observed the same behavior in the one-qubit case, where partially mixed states had a much wider 0.99-fidelity region than either of the endpoints (the one-qubit pure and fully mixed states). This is encouraging news for most quantum infomation tasks, which employ pure states.

4.2. State Concentration

While so far we have focused on the characteristics of mixed entangled states, pure maximally entangled states are generally more useful for quantum information protocols. However, maximally entangled pure states may not always be available, so it is important to study ways in which entanglement and purity may

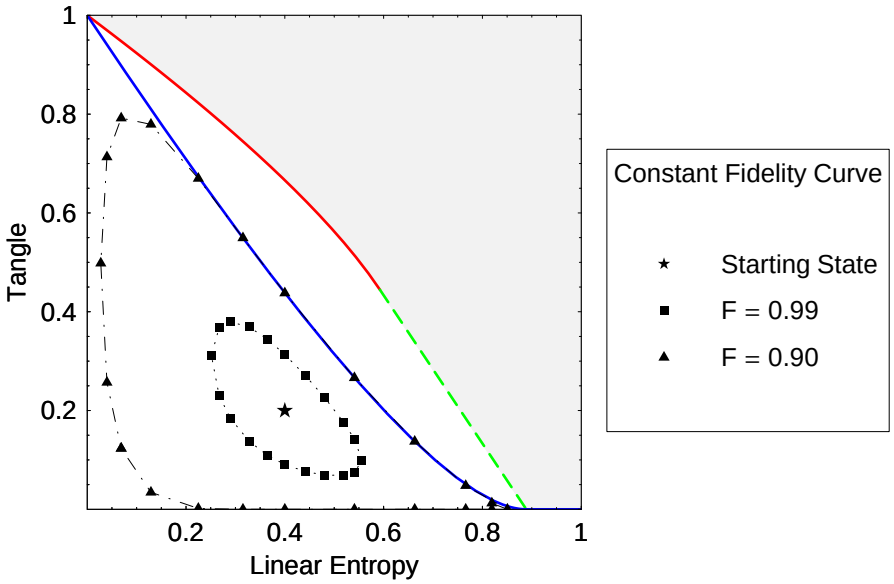

Figure 6. Constant fidelity curves for a nonmaximally entangled mixed state with $\lambda = 0.225403$ and $\theta = 11.5725°$. The constant fidelity curves are swept out by comparing the starting state with states calculated by varying λ and θ. In the case of this mixed entangled state, the constant fidelity regions are surprisingly large.

be increased by acting on the initial ensemble. Recently, several entanglement concentration[‡] experiments have been realized that exploit two-photon interference effects.[27–29] An interesting characteristic of MEMS is that they may be concentrated using "Procrustean" local filtering[30,31] in a much more efficient way than other techniques allow.[19] We have implemented a partial polarizer based Procrustean filtration technique[26,30,31] which simultaneously increases both the purity and the tangle of the MEMS by rejecting some of the pairs of the initial photon ensemble. Though this implementation requires knowledge of the state, a greater entanglement per initial state ensemble pair is achievable[19] than with other recent concentration schemes.[27–29] We first modify our MEMS with a HWP oriented at 45° in the first arm, thereby exchanging $|H\rangle \leftrightarrow |V\rangle$ in that arm. The nonzero MEMS diagonal elements then become $|HV\rangle\langle HV|$, $|VH\rangle\langle VH|$, and $|VV\rangle\langle VV|$. Reducing the $|VV\rangle\langle VV|$ element of this modified MEMS drives the state to the pure maximally entangled state $|\phi^+\rangle \equiv (|HV\rangle + |VH\rangle)/\sqrt{2}$. The filtering is achieved with partial polarizers, an implementation of a generalized positive operator value measure (POVM), made from glass pieces oriented at Brewster's angle as indicated in figure 7 (a). The orientation is such that horizontally polarized photons are nearly perfectly transmitted (with transmission probability $T_H = 0.990 \pm 0.006$) while vertically polarized photons are partially reflected ($T_V = 0.740 \pm 0.002$). Each glass piece consists of four ∼1-mm thick microscope slides sandwiched together with index matching fluid. The resulting 4-mm thickness was needed to ensure that multiple internal reflections in one piece of glass did not induce decoherence. Equal numbers of pieces are placed in each arm, and they are always used in displacement compensating pairs as shown in the figure 7 (a).

We concentrated a variety of MEMS as shown in figure 7 (b). At first, as the number of glass pieces increased, the state became more entangled and less mixed, as predicted.[26] But then we observe a reversal, indicated for various numbers of theoretical concentrating elements by stars on the figure). This behavior is not unexpected if one considers the density matrix of the state throughout the filtering process. Initially,

[‡]We adopt Thew and Munro's nomenclature[26] where "concentration" refers to a process in which a state's purity and entanglement are *both* increased.

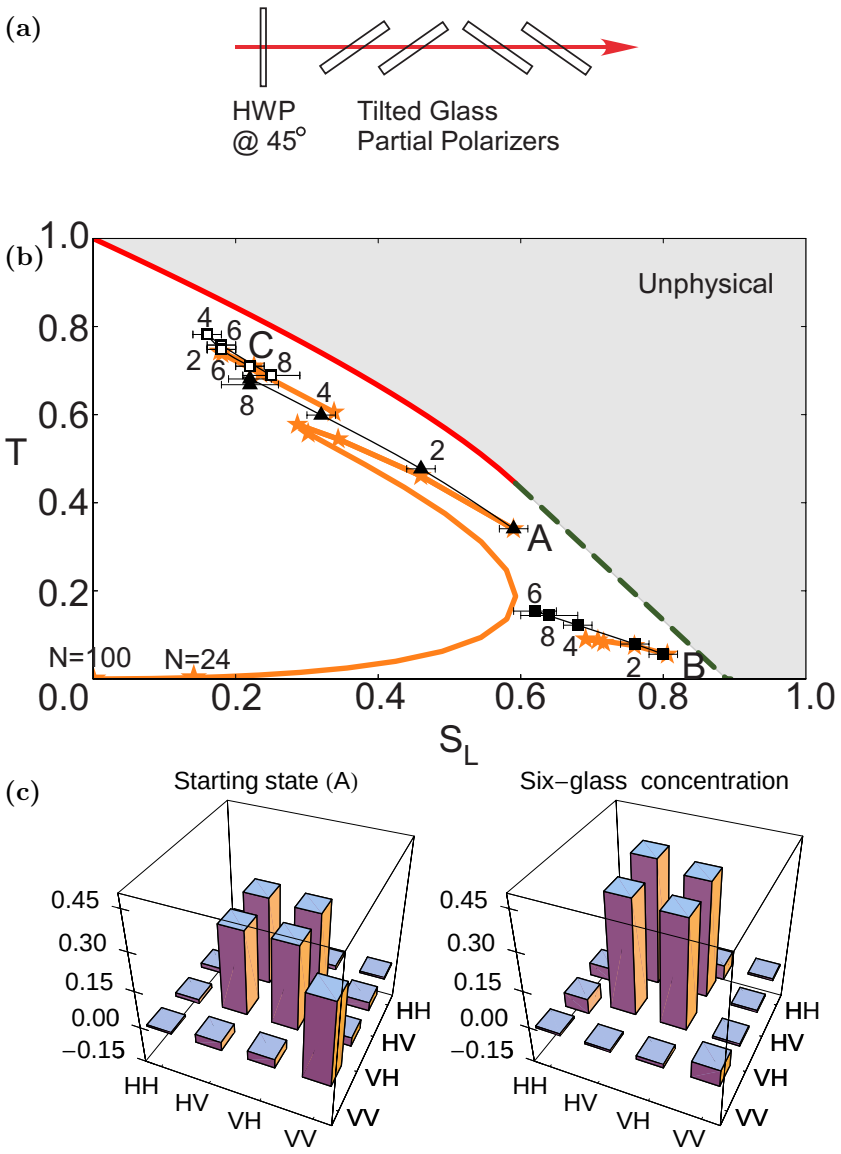

Figure 7. Concentration elements and data. (a) Elements placed after MEMS preparation and before the tomography system of figure 3. The half-waveplate, only in the top arm of the experiment, is oriented to rotate $|H\rangle \leftrightarrow |V\rangle$. Following the HWP, but located in both arms of the experiment, are the concentrating elements, a variable number of glass pieces oriented at Brewster's angle to completely transmit $|H\rangle$ but partially reflect $|V\rangle$. (b) Shown are concentrations for three initial states (triangles, filled squares, and open squares) along with the number of partial polarizing glass pieces in each arm. (Reprinted figure with permission from Ref. 19. © 2004 the American Physical Society.) The theoretical concentrated state path is shown with stars. Experimental states agree with theory for small numbers of glass pieces, but as the number increases, the states concentrate better than expected. We believe that is explained by the concentration theory's extreme sensitivity to small changes in the initial state (see figure 8). Note, however, that if there are even extremely minute errors in the "zero" diagonals of MEMS, excessive filtration will eventually produce a pure product state (shown as an extension of A's theory curve). (c) Real parts of the density matrix plots for the unconcentrated initial state (A), and for the same state after concentration using six glass pieces per experimental arm. The imaginary parts are negligible and not shown.

the MEMS we can produce in our laboratory has the three desired large diagonal values ($|HV\rangle\langle HV|$, $|VH\rangle\langle VH|$, and $|VV\rangle\langle VV|$) and one additional very small value ($|HH\rangle\langle HH|$) due to slight imperfections in the state. As concentration begins, all vertically polarized terms are reduced according to T_V; therefore $|VV\rangle\langle VV|$ is reduced twice as much as $|HV\rangle\langle HV|$ and $|VH\rangle\langle VH|$. Since horizontal transmission through the partial polarizers is nearly unity, the reduction of the $|HH\rangle\langle HH|$ term is negligible. As the $|VV\rangle\langle VV|$ element is reduced, the state initially becomes more entangled and less mixed. Eventually, however, the $|VV\rangle\langle VV|$ value will equal that of $|HH\rangle\langle HH|$, an example of a Werner state. This is where the theoretical prediction for the state starts to become *less* entangled and *more* mixed. This entanglement *un*concentration continues until the $|HH\rangle\langle HH|$ value is the same as $|HV\rangle\langle HV|$ and $|VH\rangle\langle VH|$, after which point further concentration eliminates all diagonal values that have vertical polarization terms. Consequently, extreme concentration will produce the pure product state $|HH\rangle$.

Our states tended to concentrate slightly better than the theoretical predictions. We attribute this to the extreme sensitivity of the theoretical concentration "trajectory" to the precise initial state. As our numerical simulation of Poisson perturbations on the Bell state indicated, a depolarizing channel has the same effect as Poisson noise. To study this further, we performed a theoretical calculation using (15) to show that small amounts of noise added to an initial state ($\rho_{MEMSI}(r = \frac{2}{3})$) greatly change how well it may be concentrated (see figure 8). We see that noisy states (even though they have high fidelities with the perfect $\lambda = 0$ state) vary greatly in their trajectories on the entropy-tangle plane, and also in their final concentrated forms.

5. CONCLUSIONS

We have shown that we can create a wide variety of states, including MEMS, to study noise in the context of mixed states. We examined the relative noise insensitivity of the fidelity for one-qubit mixed states and applied similar methods to investigate two-qubit states. With these methods, we explored the behavior of the entropy and tangle for states of a given fidelity with a target state. The resulting large entropy-tangle areas for "high fidelity" states indicate that the fidelity is much less sensitive than entanglement and mixedness than we previously thought. Finally, we have implemented a Procrustean concentration scheme on several MEMS, achieving a concentration efficiency higher than that available with other methods. However, slight perturbations in the initial state greatly bias the concentration outcome, and extreme filtering will only produce product states (as in figure 7 (b)). Consequently, an optimal concentration strategy may be a hybrid between Procrustean and other interference-based methods.[27–29]

ACKNOWLEDGMENTS

This work was supported by the DCI Postdoctoral Research Fellowship Program, the National Science Foundation (Grant number EIA-0121568), and the MURI Center for Photonic Quantum Information Systems (ARO/ARDA program DAAD19-03-1-0199).

REFERENCES

1. N. Gisin, G. Ribordy, W. Tittel, and H. Zbinden, "Quantum cryptography," *Rev. Mod. Phys.* **74**, p. 145, Mar. 2002.
2. *Focus Issue on Quantum Cryptography,* P. G. Kwiat, ed., New J. Phys. **4**, Jul. 2002.
3. C. H. Bennett *et al.*, "Teleporting an unknown quantum state via dual classical and Einstein-Podolsky-Rosen channels," *Phys. Rev. Lett.* **70**, p. 1895, Mar. 1993.
4. C. H. Bennett and S. J. Wiesner, "Communication via one- and two-particle operators on Einstein-Podolsky-Rosen states," *Phys. Rev. Lett.* **69**, p. 2881, Nov. 1992.
5. S. Bose and V. Vedral, "Mixedness and teleportation," *Phys. Rev. A* **61**, p. R040101, Mar. 2000.
6. R. Jozsa, "Fidelity for mixed quantum states," *J. Mod. Optics* **41**, pp. 2315–2324, Dec. 1994.
7. W. K. Wooters, "Distributed entanglement," *Phys. Rev. Lett.* **80**, p. 2245, Mar. 1998.

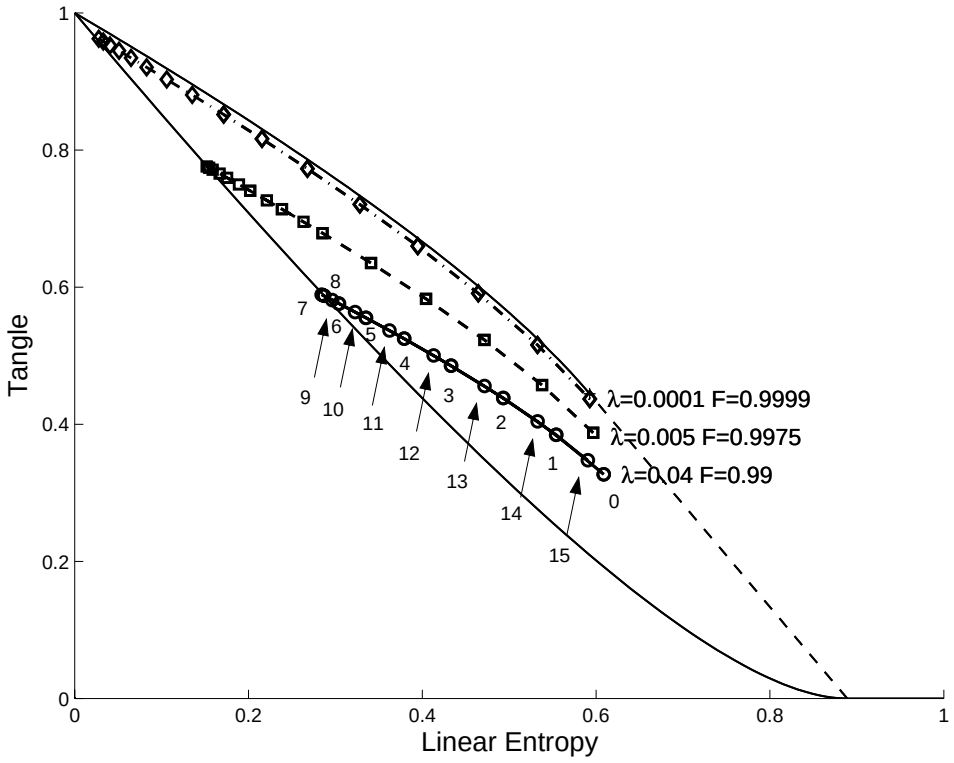

Figure 8. Investigation of the concentrate-ability of a MEMS state (nominally with $r = \frac{2}{3}$), as a function of additional noise λ. 15-step concentration calculation (corresponding to 1 to 15 glass pieces per experimental arm as in Figure 7) for $\rho_2(\lambda, r = \frac{2}{3})$. Shown are the depolarizing parameters (λ) along with the fidelity (F) of the "noisy" starting state with the ideal MEMS. Each concentration step uses the same transmission coefficients as in Figure 7. Observe that relatively small perturbations in the initial state can drastically alter its concentrate-ability. Just as in in figure 7 (b), we see that excessive concentration steps unconcentrate the state here also. For example, in the $\lambda = 0.02$ case, 1 to 7 concentrating steps increase the state's purity and tangle while the remaining steps undo the concentration. In the $\lambda = 0.0001$ case, all fifteen elements increase the tangle and purity.

8. V. Coffman, J. Kundu, and W. K. Wooters, "Distributed entanglement," *Phys. Rev. A* **61**, p. 052306, May 2000.
9. N. A. Peters *et al.*, "Precise creation, characterization and manipulation of optical qubits," *J. Quant. Inf. and Comp.* **3**, pp. 503–517, Oct. 2003.
10. C. K. Hong and L. Mandel, "Experimental realization of a localized one photon state," *Phys. Rev. Lett.* **56**, p. 58, Jan. 1986.
11. P. G. Kwiat *et al.*, "New high-intensity source of polarization-entangled photon pairs," *Phys. Rev. Lett.* **75**, p. 4337, Dec. 1995.
12. P. G. Kwiat *et al.*, "Ultrabright source of polarization-entangled photons," *Phy. Rev. A* **60**, p. R773, Aug. 1999.
13. A. G. White, D. F. V. James, P. H. Eberhard, and P. G. Kwiat, "Nonmaximally entangled states: Production, characterization, and utilization," *Phys. Rev. Lett.* **83**, p. 3103, Oct. 1999.
14. A. G. White, D. F. V. James, W. J. Munro, and P. G. Kwiat, "Exploring hilbert space: Accurate characterization of quantum information," *Phys. Rev. A* **65**, p. 012301, Dec. 2001.
15. Y. S. Zhang, Y. F. Huang, C. F. Li, and G. C. Guo, "Experimental preparation of Werner state via spontaneous parametric down-conversion," *Phys. Rev. A* **66**, p. 062315, Dec. 2002.
16. W. J. Munro, D. F. V. James, A. G. White, and P. G. Kwiat, "Maximizing the entanglement of two mixed qubits," *Phys. Rev. A* **64**, p. R030302, Aug. 2001.
17. T. C. Wei *et al.*, "Maximal entanglement versus entropy for mixed quantum states," *Phys. Rev. A* **67**, p. 022110, Feb. 2003.
18. P. Kwiat *et al.*, quant-ph/0303040, 2003.
19. N. A. Peters *et al.*, "Maximally entangled mixed states: Creation and concentration," *Phys. Rev. Lett.* To appear 2004; also quant-ph/0308003 2003.
20. D. F. V. James, P. G. Kwiat, W. J. Munro, and A. G. White, "Measurement of qubits," *Phys. Rev. A* **64**, p. 052312, Oct. 2001.
21. M. Barbieri, F. D. Martini, G. D. Nepi, and P. Mataloni, "Violation of bell inequalities and quantum tomography with pure-states, werner-states and maximally entangled mixed states created by a universal quantum entangler," *quant-ph/0303018*, 2003.
22. G. D. Nepi, F. D. Martini, M. Barbieri, and P. Mataloni, "Universal ultrabright source of entangled photon states: generation and tomographic analysis of werner states and of maximally entangled mixed states," *quant-ph/0307204*, 2003.
23. A. J. Berglund, "Quantum coherence and control in one- and two-photon optical systems," *Dartmouth College B.A. Thesis*; also *quant-ph/0010001*, 2000.
24. P. W. Shor, "Fault-tolerant quantum computation," in *Proceedings of 37th Symposium on Foundations of Computing*, pp. 56–65, IEEE Press, 1996.
25. E. Knill, R. Laflamme, and H. Zurek, "Resilient quantum computation," *Science* **279**, p. 342, Jan. 1998.
26. R. T. Thew and W. J. Munro, "Entanglement manipulation and concentration," *Phys. Rev. A* **63**, p. R030302, Feb. 2001.
27. T. Yamamoto, M. Koashi, S. K. Özdemir, and N. Imoto, "Experimental extraction of an entangled photon pair from two identically decohered pairs," *Nature* **421**, pp. 343–346, Jan. 2003.
28. J. W. Pan *et al.*, "Experimental entanglement purification of arbitrary unknown states," *Nature* **423**, pp. 417–421, May 2003.
29. Z. Zhao *et al.*, "Experimental realization of entanglement concentration and a quantum repeater," *Phys. Rev. Lett.* **90**, p. 207901, May 2003.
30. C. H. Bennett, H. J. Bernstein, S. Popescu, and B. Schumacher, "Concentrating partial entanglement by local operations," *Phys. Rev. A* **53**, p. 2046, Apr. 1996.
31. P. G. Kwiat, S. Barraza-Lopez, A. Stefanov, and N. Gisin, "Experimental entanglement distillation and 'hidden' non-locality," *Nature* **409**, p. 1014, Feb. 2001.